



Article

A Study on TGF Detectability at 2165 m Altitude: Estimates for the Mountain-Based Gamma-Flash Experiment

Alessandro Ursi ^{1,*} , Gonzalo Rodriguez Fernandez ² , Alessandra Tiberia ³ , Enrico Virgilli ⁴ ,
Enrico Arnone ⁵ , Enrico Preziosi ⁶ , Riccardo Campana ⁴ and Marco Tavani ^{1,2}

¹ Institute for Space Astrophysics and Planetology (IAPS)-National Institute for Astrophysics (INAF), National Institute for Astrophysics, I-00133 Rome, Italy; marco.tavani@inaf.it

² Dipartimento di Fisica, Università di Roma "Tor Vergata", I-00133 Rome, Italy; gonzalo.rodriguez@uniroma2.it

³ Institute of Atmospheric Sciences and Climate (ISAC)-National Research Council (CNR), Institute for Atmospheric Science and Climate, I-00133 Rome, Italy; alessandra.tiberia@artov.isac.cnr.it

⁴ Astrophysics and Space Science Observatory (OAS)-National Institute for Astrophysics (INAF), National Institute for Astrophysics, I-4012 Bologna, Italy; enrico.virgilli@inaf.it (E.V.); riccardo.campana@inaf.it (R.C.)

⁵ Dipartimento di Fisica, Università di Torino, I-10124 Turin, Italy; enrico.arnone@unito.it

⁶ Physics Department and NAST Centre, Università di Roma "Tor Vergata", I-00133 Rome, Italy; enrico.preziosi@uniroma2.it

* Correspondence: alessandro.ursi@inaf.it

Abstract: Gamma-Flash is an Italian program devoted to the realization of both a ground-based and an airborne gamma-ray and neutron detection system, for in situ measurements of high-energy phenomena correlated to thunderstorm activity, such as Terrestrial Gamma-ray Flashes (TGFs), gamma-ray glows, and associated neutron emissions. The ground-based Gamma-Flash experiment is currently under installation at the Osservatorio Climatico "Ottavio Vittori" (CNR-ISAC) on Mt. Cimone, in Northern-Central Italy (2165 m a.s.l.), and it will be operational starting in Summer 2022. We studied the detectability of TGFs in the surroundings of the ground-based Gamma-Flash experiment, to identify an investigable spatial region around the detectors from which typical TGFs can survive and be revealed onground. We carried out numerical simulations of gamma-ray propagation in the mid-latitude atmosphere, and we developed a qualitative analytical model to integrate the results. This analysis allows one to identify a spatial region extending up to 4 km distance on ground and up to 10 km altitude a.s.l., considering typical TGFs emitting $\sim 10^{18}$ gamma-ray photons at the source. Lightning sferics data acquired by the LINET network demonstrate that such a region is interested by frequent cloud-to-ground and intra-cloud lightning, pointing out the suitability of the location for the purposes of the Gamma-Flash program.

Keywords: terrestrial gamma-ray flashes; lightning; high-energy radiation



Citation: Ursi, A.; Rodriguez Fernandez, G.; Tiberia, A.; Virgilli, E.; Arnone, E.; Preziosi, E.; Campana, R.; Tavani, M. A Study on TGF Detectability at 2165 m Altitude: Estimates for the Mountain-Based Gamma-Flash Experiment. *Remote Sens.* **2022**, *14*, 3103. <https://doi.org/10.3390/rs14133103>

Academic Editors: Stefano Federico, Gaopeng Lu, Yang Zhang and Fanchao Lyu

Received: 24 May 2022

Accepted: 23 June 2022

Published: 28 June 2022

Publisher's Note: MDPI stays neutral with regard to jurisdictional claims in published maps and institutional affiliations.



Copyright: © 2022 by the authors. Licensee MDPI, Basel, Switzerland. This article is an open access article distributed under the terms and conditions of the Creative Commons Attribution (CC BY) license (<https://creativecommons.org/licenses/by/4.0/>).

1. Introduction

According to the current theories [1,2], Terrestrial Gamma-ray Flashes (TGFs) may take place at different altitudes inside the parent thundercloud and propagate toward different directions, making them detectable also on the ground or in air nearby the thunderstorm regions. In recent years, a growing number of observations of TGFs and other thunderstorm-related high-energy emissions at lower altitudes has been reported, including detections in the air by instruments placed onboard aircraft passing nearby typical thunderstorms [3] or hurricane [4], and on the ground by facilities for the detection of high-energy radiation and particles, from both natural [5–11] and rocket-triggered lightning [12–14]. Moreover, the recent discovery of "reverse positron beam TGFs" [15,16] suggests that these events may be indirectly detectable also in the opposite direction to that traveled by the electronic Bremsstrahlung radiation, making typical upward TGFs also detectable from the ground, under particular energetic and geometrical circumstances. Onground facilities aimed at the

detection of TGFs often also reveal minute-lasting high-energy emissions, named gamma-ray glows [17–20]. In some cases, even the emission of neutrons has been detected [7,8], originating from photonuclear reactions in the atmosphere triggered by the TGF gamma-ray radiation interacting with ^{14}N nuclei. Detection of neutron emissions from thunderstorms at Mt. Aragosta and other high altitude sites [21,22] and lack of detection at lower altitude [23] support the choice of our experimental site and the need for simulating their detectability.

1.1. The Gamma-Flash Program

Gamma-Flash is an Italian program devoted to the study of radiation and particle properties in lightning and thunderstorms. It is funded by the Italian Space Agency (ASI) and led by the National Institute for Astrophysics (INAF), with the collaboration of numerous institutions and universities, such as the Institute for Atmospheric Science and Climate (CNR-ISAC), the National Institute of Nuclear Physics (INFN), the NAST Centre and the University of Rome “Tor Vergata”, the University of Padua, and the Inter-University Consortium for Space Physics (CIFS). The aim of the program is the development of two innovative suites, both including gamma-ray and neutron detectors, the former to be placed onground and the latter on aircraft, to perform either onground and in-flight measurements of high-energy radiation emissions from thunderstorms. The main target of Gamma-Flash is the investigation of high-energy emissions in thunderstorms, which may lead to a substantial impact in many fields of research where these processes are as yet not considered, such as local and global climate change, natural hazard studies, and atmospheric plasma physics. The Gamma-Flash suite of detectors is designed to detect both short-duration transients (i.e., TGFs), as well as minute-lasting gamma-ray emissions (i.e., gamma-ray glows) and associated high-energy particle emissions (e.g., neutrons). Moreover, the experiment is also aimed at estimating the susceptibility of electronic devices and systems to TGF-induced ionizing radiation and particles, using a set of non-volatile semiconductor memories, whose chip information would be corrupted proportionally to the flux of ionizing gamma-rays and neutrons hitting the cells. The investigation of thunderstorm-related high-energy emissions will be supported by a continuous monitoring of the associated atmospheric scenario, by means of meteorological data analyzed on a local scale (e.g., data acquired by low Earth orbit, or geostationary satellites), and by low-light cameras for the observations of lightning processes above the clouds. The Gamma-Flash team is a world leader group in the field of TGF studies, atmospheric physics, high-energy particle and radiation instruments, radiation damage, data analysis, and simulations, taking advantage of the more than ten years experience acquired by the AGILE satellite [24–33], jointly with the ground-based LINET lightning research capability of the CNR-ISAC. The mountain-based Gamma-Flash experiment is currently in its installation phase, and it will be operational starting from Summer 2022.

1.2. The Ground-Based Gamma-Flash Detection System

In this work, we focus on the mountain-based Gamma-Flash detection system, which is currently under installation at the Osservatorio Climatico “Ottavio Vittori” (CNR-ISAC), the only Global Atmospheric Watch—World Meteorological Organization (GAW-WMO) station in Italy, sited on the top of Mt. Cimone ($44^{\circ}11'35.3544''\text{N}$; $10^{\circ}42'4.9032''\text{E}$; 2165 m a.s.l.). From the peak of Mt. Cimone, it is possible to have a free line of sight observing up to 40% of the Italian territories, making it an ideal site to carry out meteorological and atmospheric observations. This geographic region is interested by frequent lightning activity and associated detection of Transient Luminous Event (TLEs) [34], making it a suitable location for the installation of instrumentation for the detection of thunderstorm-related high-energy phenomena. The Gamma-Flash suite of gamma-ray and neutron detectors is under installation on the external terrace of the observatory, inside an aluminium naval dome of 126 cm diameter to prevent it from weather issues, such as wind, rain, snow, and ice.

1.3. TGF Detectability at Mt. Cimone

In this perspective, it is essential to investigate the geographic region where the detectors are being installed, in order to verify how suitable the location is for the detection of TGFs. This evaluation is carried out in two steps. Firstly, a study of the atmospheric gamma-ray optical depth (i.e., the distance a given radiation survives up to in a medium) in the spatial region surrounding the Gamma-Flash detectors, in order to establish a set of positions (or volume) nearby the installation site from which a typical TGF should be detected onground, what we define “detectability region”: this allows us to evaluate how far a TGF event can occur from the detection system, to be revealed and analyzed, considering different geometrical configurations and emission parameters. Secondly, a study of the lightning activity in the Mt. Cimone geographic region, using lightning network data, aimed at quantifying the yearly local occurrence of lightning flashes in the detectability region obtained in the first step: this allows us to provide an estimate of the number of expected lightning discharges in the region of interest, which will be somehow proportional to the number of expected TGFs.

2. Methods

The number of gamma-ray photons survived at the detector height dramatically depends on the radiation-matter interaction undergone in the atmosphere, and on several other factors, such as: the environmental gamma-ray background present at the site, the number of initial gamma-ray photons produced at the source, as well as their spectral energy distribution, the source position with respect to the target, the gamma-ray emission angle, the collecting area adopted to reveal the survived photons, and the density and material of the traveled medium. All these parameters should be taken into consideration in order to set up either numerical simulations or analytical treatments. In this study, we do not focus on quantifying the gamma-ray flux surviving from the TGF source to the Gamma-Flash detectors, but we are mostly interested in identifying the extent of the detectability region in the surroundings of the installation site, within which potential TGF events could be detected onground.

2.1. Gamma-ray Signal and Environmental Background

In order to identify a TGF signal in the Gamma-Flash data, it is fundamental to assess the natural gamma-ray background present at the installation site. A substantial environmental gamma-ray count rate would affect the signal-to-noise ratio (SNR), requiring the imposition of a proper threshold to discriminate gamma-ray signals from the background noise. The typical average background rate at the Gamma-Flash installation site, evaluated during a preliminary survey, is equal to 110–120 Hz, in the 100 keV–10 MeV energy range. This value, on the typical TGF timescales (i.e., few tens - few hundreds of microseconds), translates into a rate of 10^{-4} Hz, which therefore does not affect the SNR. The natural gamma-ray background does not play a role in the identification of TGF signals in the Gamma-Flash data: even a very far TGF, for which only a small fraction of gamma-ray photons survives to the detector, would be easily distinguishable above the background. For instance, an event releasing only 2 or 3 counts within the same 500 μ s bin would result in a significance of $>8\sigma$ or $>10\sigma$ above a 0.05 counts/bin background rate, respectively. Nonetheless, we point out that the true nature of a TGF is not only established on the basis of its count rate, but also by cross-searching simultaneous radio signals in the lightning data from external lightning networks: a bunch of gamma-ray photons occurring in coincidence with a VLF sferic detected by an external lightning detection system would provide a hint that such a gamma-ray signature could constitute a TGF emission. In this case, the lightning rate should also be considered, in order to evaluate the corresponding post-trial probability of a genuine correlation and rule out chance coincidences. The same applies, taking into consideration other sources of fake events (i.e., electronic noise, cosmic rays). We therefore do not ask our simulations to provide a number of survived photons exceeding a given

threshold, but we consider that all the positions for the number of survived photons at the detector is greater than zero.

2.2. Number of Seeds

The number of seeds N_0 is the initial number of gamma-ray photons produced by the TGF at the source. Typically, a TGF is expected to produce an average number of $\sim 10^{18}$ gamma-ray photons [35,36], with about $\sim 10^{17}$ photons with energies above 1 MeV [2], but some detections are compatible with lower numbers of initial photons [6], or even with larger values [10]. This parameter is the starting point of the analysis and it should be carefully managed, as it could imply computational constraints when dealing with numerical simulations.

2.3. Source Position

The position of the source with respect to the target determines the distance traveled by the gamma-ray photons, which dramatically affects the amount of scattering and absorption undergone by the radiation beam along its path in the atmosphere. We investigate the spatial region around the mountain-based Gamma-Flash experiment, to establish how far a TGF could be emitted from the detectors, in order to survive and be revealed. We define such spatial region with the parameters L (i.e., distance on ground from the detectors) and H (i.e., height with respect to sea level). Each set of (L, H) parameters is considered as a potential TGF source, placed at a given distance from the Gamma-Flash detectors. For each position, we investigated whether a TGF gamma-ray radiation would survive up to the Gamma-Flash detectors. In particular, we adopted a grid with L ranging from 0.0 km to 10.0 km and H ranging from 2.5 km to 15.5 km (compatible with the typical troposphere altitude at mid-latitudes), both ticked at steps of 500 m, as shown in Figure 1, for a total number of 567 potential TGF positions.

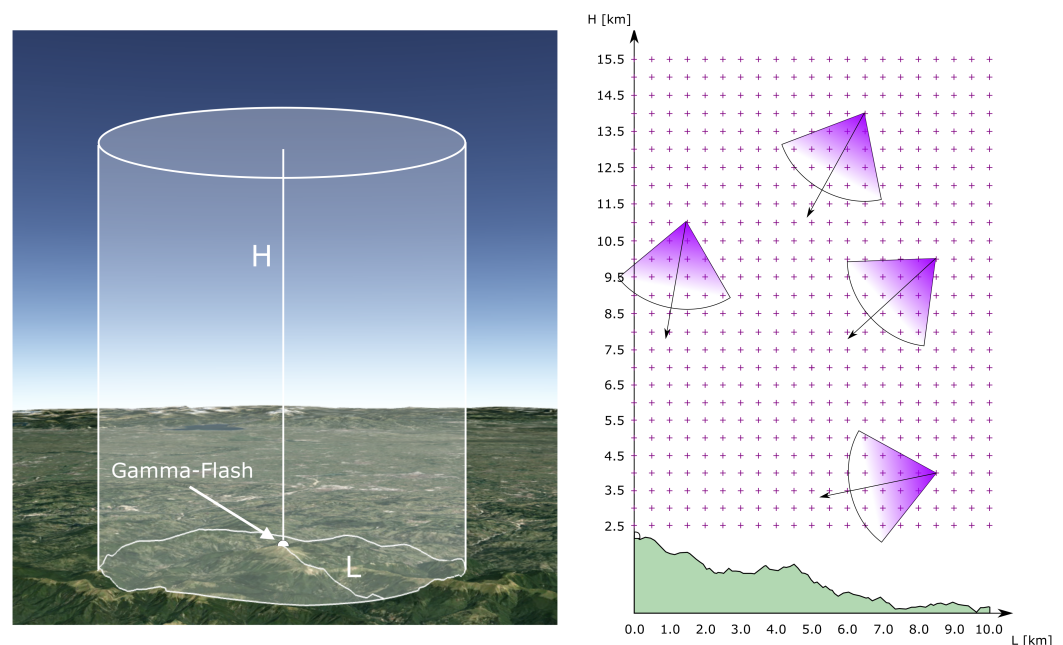


Figure 1. Left: spatial volume (white shaded) around the ground-based Gamma-Flash experiment installed on the top of Mt. Cimone (white dome), considered to evaluate the detectability region for the potential detection of TGFs. Distances on ground range within 0.0–10.0 km from the detector, and altitudes range within 2.5–15.5 km a.s.l. Right: schematic view of all the (L, H) potential TGF source positions (purple crosses) considered for the analysis. For all positions, we simulate TGFs characterized by emission half-angles $\alpha = 40^\circ$ (purple shaded), all directed toward the Gamma-Flash detectors in $(L, H) = (0.0 \text{ km}, 2.5 \text{ km})$ (white dome).

2.4. Beaming and Direction

TGFs are thought to consist of beamed gamma-ray emissions, with half-angles mostly compatible with 30–40°, according to [37]. Above 40°, the broad emission angles would make TGFs experience a much larger absorption, resulting in a substantial softening, or suppression, of the gamma-ray flux. On the other hand, tighter emission angles would produce harder spectrum TGFs at the detector, although making them less easily detectable, due to geometric issues. In our simulations, we generate each TGF event as a number of N_0 initial seeds emitted within a half-angle $\alpha = 40^\circ$. Moreover, each TGF emission cone was simulated pointing directly toward the Gamma-Flash detectors. A schematic representation is shown in Figure 1.

We point out that this analysis is only aimed at the evaluation of the TGF detectability by the Gamma-Flash mountain-based detectors: for this reason, the approach philosophy is to investigate the most favorable geometric conditions of emission angle and pointing direction, with respect to the experimental set-up. If the flux of a TGF occurring at a given position (L, H) does not survive to the detector, even in the most favorable geometric conditions (i.e., directly pointing toward the target), we can confidently consider such point a non-investigable position for the Gamma-Flash experiment.

2.5. Collecting Area

In order to evaluate the number of survived photons, it is necessary to establish a collecting area in which such photons shall be counted. In particular, we want to assess how the number of survived TGF photons at ground changes, with changing the size of the collecting surface, in order to establish how these photons distribute at the ground. We considered different collecting areas, centered around the ground-based Gamma-Flash position. In particular, we adopted circular areas with radii $r_{coll} = 250$ m, 100 m, 10 m, 63 cm, and 10 cm. The 63 cm area corresponds to the basis surface of the naval dome housing the Gamma-Flash detectors on the external terrace of the observatory, whereas the 10 cm area roughly corresponds to the total geometric area of the gamma-ray detectors.

2.6. Medium Density and Material

The density and material of the medium in which the gamma-ray photons propagate plays a fundamental role in the radiation-matter interaction and in how this affects the final flux of gamma-ray photons, after undergoing absorption and scattering. In order to describe the atmospheric density, we adopted the U.S. Standard Atmosphere [38], which is one of the most common atmospheric density models. It assumes a constant mean molecular weight consisting in 80% N_2 and 20% O_2 , providing reliable values up to 86 km altitude. The model describes the density profile as a function of altitude $\rho(H)$, exponentially decreasing as:

$$\rho(H) = \rho_0 e^{-\frac{H-H_0}{h_0}} \quad (1)$$

where $\rho_0 = 1.255 \text{ kg/m}^3$ is the reference density at sea level, $H_0 = 0$ m is the reference altitude associated to the reference density, and $h_0 \sim 8500$ m is the mean scale height of Earth atmosphere at mid-latitudes (over the range from 0 to 100 km). We point out that the scale height value may vary, as it depends on the vertical thermal gradient present in the atmosphere, which can change depending on the ongoing meteorological conditions and associated atmospheric temperature. As a consequence, considering an isothermal atmosphere with scale heights $h_0 = RT/g$, where R is the ideal gas constant and g is the acceleration of gravity, the scale height could go from $h_0 \sim 6500$ m at 220 K (high troposphere) to $h_0 \sim 8500$ m at 280 K (near the surface). Here, we adopt the mean scale height $h_0 = 8500$ m, which better reflects our operational conditions.

Given the density profile exponentially decreasing with altitude H , the mass content in the surroundings of the Gamma-Flash installation site exhibits a peculiar “egg shape”, when considering integrated air columns with 1 m^2 unit surfaces along the beam connecting the target detector to the different nearby positions, as shown in Figure 2. As a consequence,

a beam of gamma-ray photons occurring right above the Gamma-Flash experiment, which is placed in $(L, H) = (0.0 \text{ km}, 0.0 \text{ km})$, would cross a lower amount of atmospheric air to reach the detector, with respect to a beam taking place at very large distances L , providing an atmospheric optical depth extending deeper in altitude H , rather than in distance L . As the gamma-ray-survived flux at the detector is inversely proportional to the amount of matter traveled by the radiation, we expect a typical ground facility to be more sensitive to TGFs taking place right above the installation site, rather than at very large side L distances.

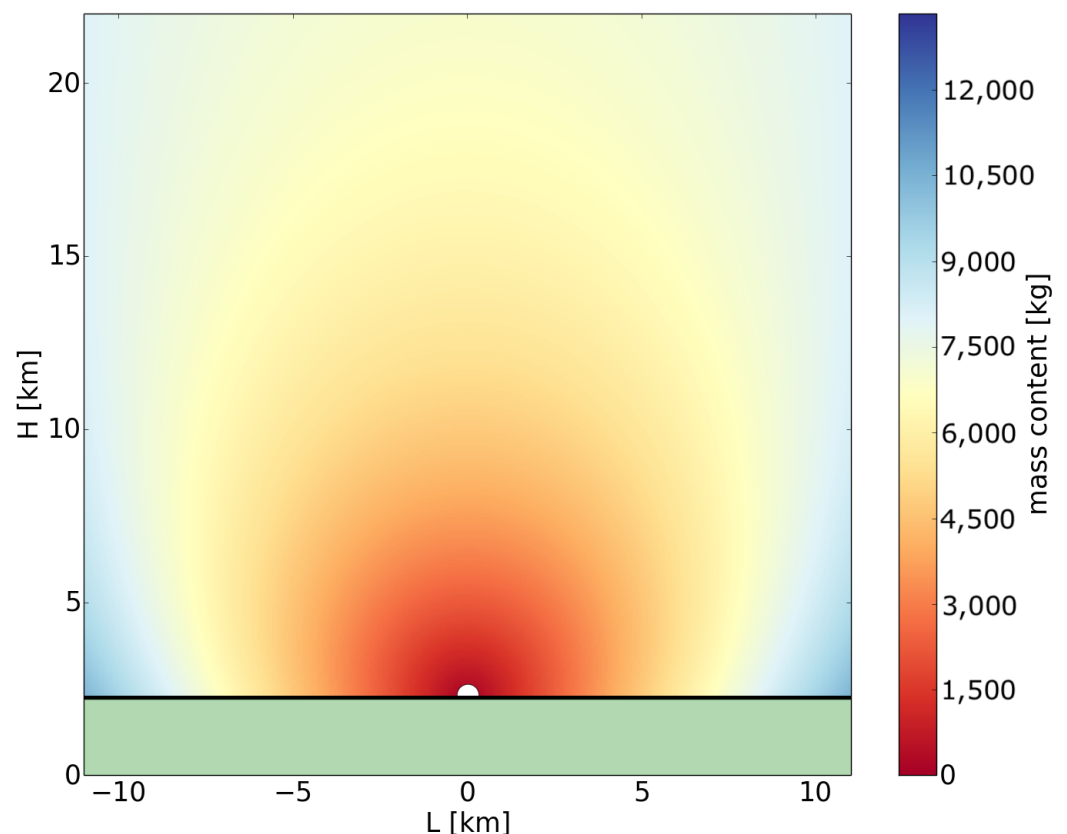


Figure 2. Atmospheric mass content in the surroundings of the Gamma-Flash ground-based experiment (white dome), obtained by evaluating the amount of matter contained in a unitary column going from $(L, H) = (0.0 \text{ km}, 0.0 \text{ km})$ to the surrounding positions. As the atmospheric density profile decreases exponentially with altitude H , the distribution assumes an “egg shape”, making the mass content higher if moving along L , rather than along H .

2.7. Energy Spectrum

For the energy density distribution of photons at the source, we used the typical TGF spectrum proposed by [39], which consists in a cutoff power-law with energy break at $E \sim 6.6 \text{ MeV}$. In this model, the differential number of counts per unit energy dN/dE is described by:

$$\frac{dN}{dE} = KE^{-1} e^{-\frac{E}{6.6 \text{ MeV}}} \quad (2)$$

where K is a normalization constant. As pointed out in [40], the spectrum plays a crucial role in estimating the number of survived photons at the target. Due to the dependence of the radiation cross-section, and radiation-matter interaction, on energy, different spectral energy distributions would result in different survived fluxes, strongly affecting the TGF detectability of a given gamma-ray detection facility. Here, we only consider the “standard” TGF spectrum, in order to estimate how far a typical event can be detected.

3. Monte Carlo Simulations

We carried out Geant4 [41–43] simulations of gamma-ray photons propagation in the atmosphere. We generated a number of N_0 initial gamma-ray seeds produced at each (L, H) position and analyzed the number of survived photons at the ground, from each source position, within different collecting areas. For computational constraints, we could not simulate a number of initial seeds equal to 10^{18} , expected in literature from a typical TGF. However, as the Geant4 simulated photons are independent one from each other, we adopted a number of initial seeds equal to $N_0 = 10^{10}$, with the intent of rescaling the number of survived photons by a factor 8 in a second stage.

Spatial Distribution of Survived Photons

A TGF with a fixed emission half-angle of $\alpha = 40^\circ$ would cover different surfaces on the ground depending on the initial source position (L, H) . In particular, TGFs occurring at high altitudes and at large distances would span larger surfaces on the ground, exhibiting lower overall intensities, as a result of wider projection effects. In Figure 3, we report examples of the spatial distributions at ground of simulated TGFs with $N_0 = 10^{10}$ taking place at positions $(L, H) = (0.0 \text{ km}, 2.5 \text{ km})$, $(L, H) = (2.5 \text{ km}, 2.5 \text{ km})$, $(L, H) = (0.0 \text{ km}, 5.0 \text{ km})$, and $(L, H) = (2.5 \text{ km}, 5.0 \text{ km})$, each plot with the corresponding 1σ , 2σ , and 3σ of the distribution. Depending on geometry and distance, the survived gamma-ray photons at the ground can cover huge areas, up to more than 5.0 km^2 , already for $N_0 = 10^{10}$. From the right panels of Figure 3, representing TGFs taking place at positions shifted of $L = 2.5 \text{ km}$ with respect to the detectors' installation site, it can be observed that, given the relatively large emission angles, the peak of the survived flux always lays below the source position (L, H) , rather than at the target point, due to the lower radiation-matter interaction undergone in the shorter path from source to ground. As we are not interested in the overall number of survived TGF photons at the ground, but only in those reaching the target surfaces centered at $(L, H) = (0.0 \text{ km}, 0.0 \text{ km})$, we point out that events taking place at small L values will result in larger survived fluxes at the detector, with respect to events occurring at very large side distances L , favoring the detection of TGFs occurring right above the installation site rather than at large distances L . Such behavior is compatible with the atmospheric mass content profile in the surroundings of the installation site, already pointed out in Section 2.6 and in Figure 2.

For each collecting area, we end up with a given amount of survived gamma-ray photons at the ground, originating from each (L, H) simulated position, as shown in Figure 4. For the largest collecting area ($r_{coll} = 250 \text{ m}$), gamma-ray photons may survive to the ground if produced at positions up to $L = 5.0 \text{ km}$ and up to altitudes $H = 8.0 \text{ km}$, as shown in the first panel of the figure. On the other hand, for the collecting area with $r_{coll} = 63 \text{ cm}$, a reliable statistic is obtained only for $L = 0.0 \text{ km}$ and up to $H = 3.0 \text{ km}$, as shown in the fourth panel of the figure, whereas for the smallest area with $r_{coll} = 10 \text{ cm}$ no photons are expected to survive to the detector.

These results are obtained for a number of seeds $N_0 = 10^{10}$, which is not representative of a typical TGF, and which should be rescaled by a factor of 8, in order to simulate a more realistic TGF emission. However, we point out that if, for a given source position, the number of survived photons is equal to zero for $N_0 = 10^{10}$; this value cannot be properly rescaled to $N_0 = 10^{18}$: in all these cases, the absence of survived gamma-ray photons obtained after rescaling could not be solidly ascribed to absorption in the atmosphere, or simply to the lack of statistics. The same applies for low number of survived photons, which cannot be properly rescaled, as the results would be affected by very large associated errors. As illustrated in Section 2, the main focus of this work is the definition of the spatial region around the detectors from which TGFs can be revealed, rather than the quantification of the survived fluxes: for this reason, we develop an alternative approach to integrate these results, addressed in the following section.

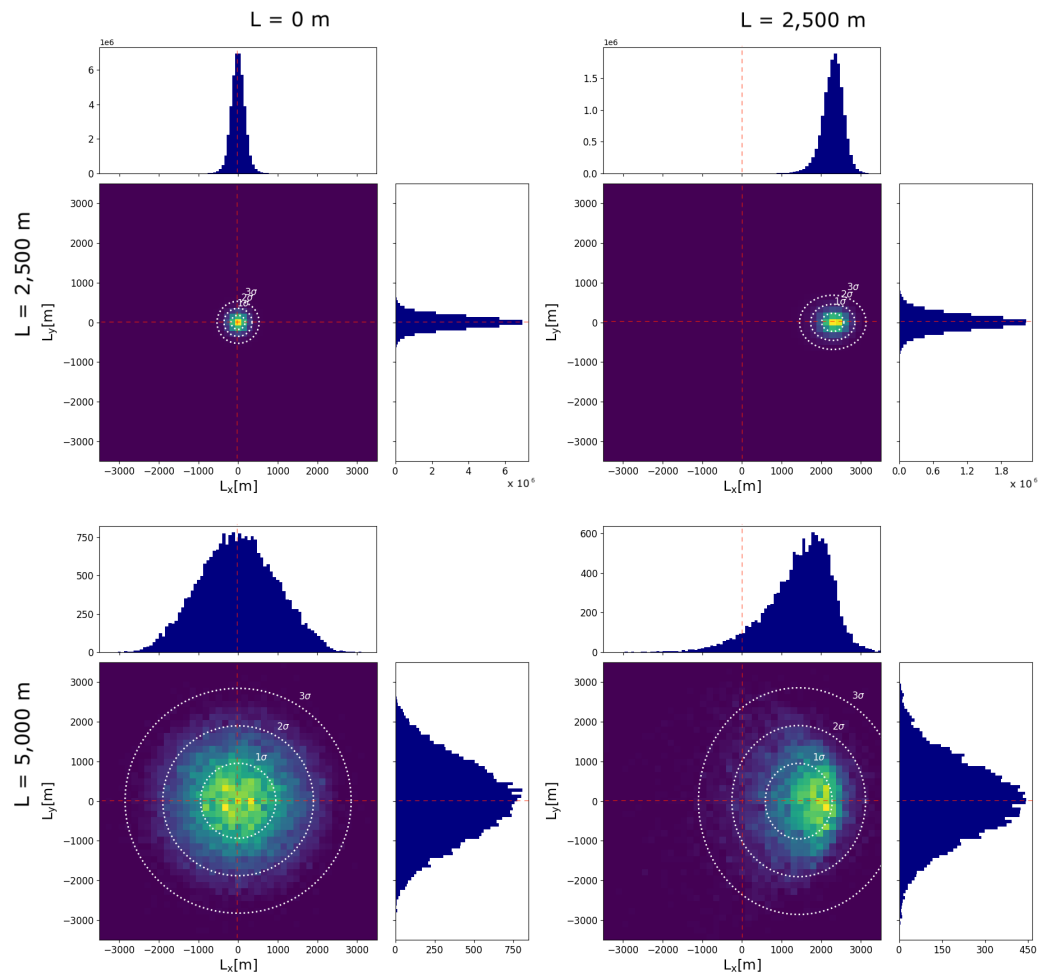


Figure 3. Spatial distribution at Mt. Cimone (2,165 m altitude) of TGF gamma-ray photons emitted at positions $(L, H) = (0.0 \text{ km}, 2.5 \text{ km})$, $(L, H) = (2.5 \text{ km}, 2.5 \text{ km})$, $(L, H) = (0.0 \text{ km}, 5.0 \text{ km})$, and $(L, H) = (2.5 \text{ km}, 5.0 \text{ km})$. Corresponding 1σ , 2σ , and 3σ of the distribution are reported for each plot. The red dashed lines indicate the position of Gamma-Flash, located in $(L, H) = (0.0 \text{ km}, 0.0 \text{ km})$. It is interesting to notice that, given the large emission angles, the peak of the survived flux always lays below the source position (L, H) , rather than at the target point placed in $(L, H) = (0.0 \text{ km}, 0.0 \text{ km})$.

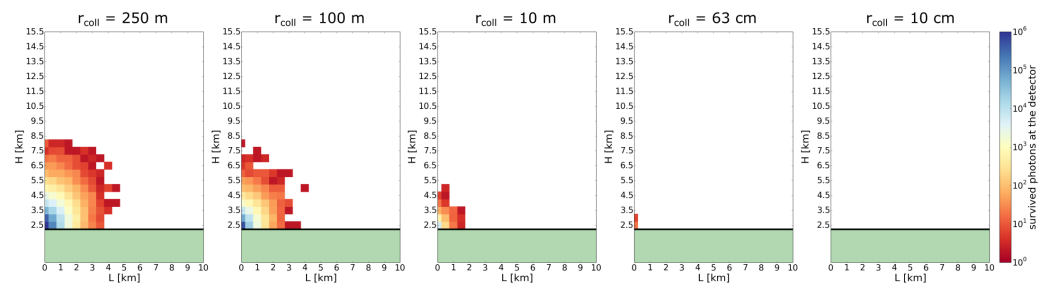


Figure 4. Detectability regions obtained from the Geant4 simulations. In the panels, the color of each (L, H) pixel represents the number of gamma-ray photons reaching a collecting area of radius r_{coll} , survived from a TGF with $N_0 = 10^{10}$ initial gamma-ray seeds emitted in that (L, H) position. The black line with the green region indicates the separation with the ground surface on Mt. Cimone, at about 2165 m a.s.l.

4. Analytical Treatment

Given the computational limitations that prevent a comprehensive numerical simulation of 10^{18} seeds at the source, we developed an analytical model to evaluate the

gamma-ray absorption of a TGF emission, traveling a given path in the atmosphere from the source to the detector. For this treatment, we adopted the same standard atmospheric density model illustrated in Section 2.6 and the same TGF spectral model used for the simulations, presented in Section 2.7. We first test this analytical treatment by carrying out the same analysis performed with Geant4, using 10^{10} initial gamma-ray photons. Once this approach is validated, we can expand N_0 to 10^{18} and evaluate the results.

We limit the number of initial gamma-ray seeds N_0 , emitted within an emission angle $\alpha = 40^\circ$, only to those directly subtending the area of interest, laying within a sub-angle $\delta\alpha$, that we name δN_0 , as schematically shown in Figure 5. The ratio between the number of emitted photons and the corresponding solid angle within which they are emitted is constant. As a consequence, the number of photons directly pointing toward the collecting area is equal to:

$$\delta N_0 = \frac{N_0 \cdot \sin^2 \delta\alpha}{\sin^2 \alpha} \tag{3}$$

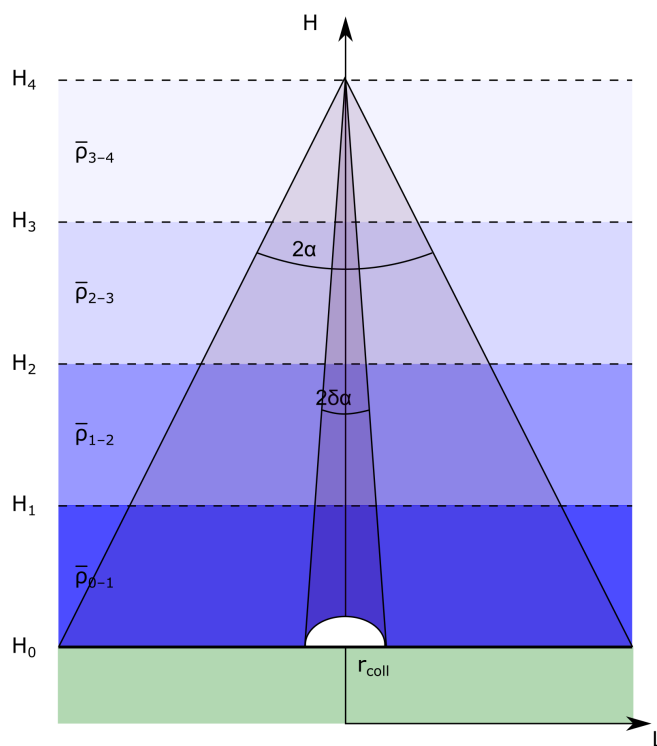


Figure 5. Schematic (L, H) diagram of a total TGF emission, inside a half-angle $\alpha = 40^\circ$, and of its related sub-half-angle $\delta\alpha$, directly subtending the collecting area under analysis (here, the surface of the dome housing the Gamma-Flash detectors, with radius $r_{coll} = 63$ cm). Radiation traveling from source to target crosses different atmospheric layers at different altitudes H , with different average densities $\bar{\rho}(H)$ (shaded regions), and undergoes different amounts of radiation-matter interaction.

This selection is brutal, as it does not take into account all those scattering processes that may deflect gamma-ray photons from their initial path, as well as all those photons that may be deflected inside the emission cone, and it can affect the obtained number of survived photons. However, it provides a qualitative evaluation of the order of magnitude of the survived photons, needed to characterize the detectability region. We adopted a number of initial seeds equal to $N_0 = 10^{10}$, in order to be consistent to the results obtained with the Geant4 simulations and cross-checked our results.

A narrow beam of high-energy photons with an incident intensity I_0 , traveling a distance R within a layer of a material with density ρ , emerges with an intensity $I(R)$ equal to:

$$I(R) = I_0 e^{-\xi\rho R} \tag{4}$$

where $\xi = \mu/\rho$ is the mass attenuation coefficient and corresponds to the linear attenuation μ per unit mass, which takes into account all the major radiation-matter interactions underwent by high-energy photons along its path in a given material (i.e., photoelectric absorption, Compton scattering, and pair production). The quantity ρR is the area density, corresponding to the mass thickness of the traveled medium. We retrieved the mass attenuation coefficient ξ for air from the National Institute for Standards and Technology (NIST) (<https://www.nist.gov/>, accessed on 21 December 2021).

Before adopting this approach to evaluate the absorption undergone by TGF radiation in the atmosphere, it is fundamental to notice a few points: first, air density is not constant and varies exponentially as a function of altitude $\rho(H)$, as already reported in Equation (1); then, the mass attenuation coefficient depends on energy as $\xi(E)$, implying different amounts of absorption for TGF photons with different energies. These considerations point out that a comprehensive estimate of the number of survived gamma-ray photons coming from a given position (L, H) should take into consideration all the different atmospheric layers encountered by the beam along its path from H to the target, featuring different densities and absorption coefficients, and it should be integrated on the corresponding total spectral energy range ΔE in which the detectors are sensitive. Considering a number n_l of atmospheric layers l , each characterized by an average density $\bar{\rho}_l$, and a number n_E of spectral energy channels E , each characterized by a given mass attenuation $\xi(E)$, we can express the number of survived photons δN_{surv} as a function of distance on ground L and altitude H :

$$\delta N_{surv}(L, H) = \sum_E^{n_E} \delta N_{0E} \prod_{l=0}^{n_l} e^{-\xi_E \bar{\rho}_l R(L, H)} \quad (5)$$

The source position (L, H) and the adopted half-angle determine the geometry of the process, as well as the number of crossed atmospheric layers to be taken into account for the mass attenuation total estimate. Here, the number of adopted atmospheric layers is $n_l = 27$, evaluated from 2.5 km to 15.5 km at steps of 500 m, whereas the number of spectral channels is the $n_E = 22$, provided by the values reported by the NIST.

Spatial Distribution of Survived Photons

The results from the analytical treatment are shown in Figure 6, where we adopt the same spatial grid used for the simulations, and evaluate the number of survived photons on the same collecting areas. We compared the results obtained for $N_0 = 10^{10}$ from the Geant4 simulations to those obtained with the analytical model, and we found a good agreement between the two approaches, as shown in Figure 7, where we report the detectability regions obtained from the simulations (red line) and the analytical treatment (blue line), for each collecting area. Although the spatial distributions obtained with Geant4 show a more jagged boundary profile, due to the presence of statistical fluctuations in the Monte Carlo simulations, we point out that the two approaches lead to the identification of very similar spatial regions around the detectors, with an average error <1.5 km, as shown in Figure 7. We point out that the distributions of survived photons exhibit larger atmospheric optical depths moving along altitude H with respect to the optical depths moving along lateral distance L , which is totally compatible with the atmospheric mass content density already shown in Section 2.6 and Figure 2.

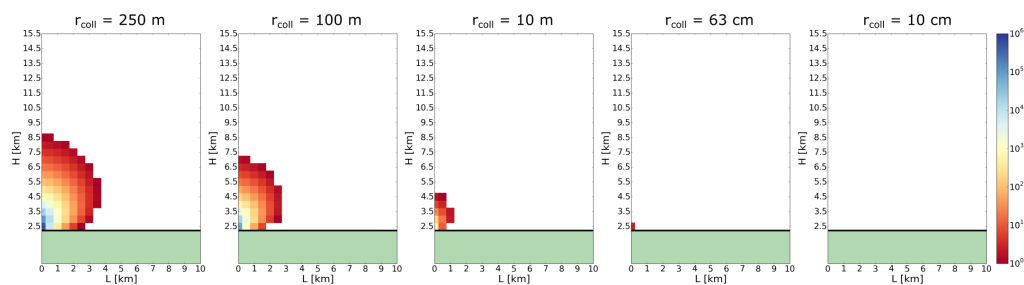


Figure 6. Detectability regions obtained from the analytical model. In the panels, the color of each (L, H) pixel represents the number of gamma-ray photons reaching a collecting area of radius r_{coll} , survived from a TGF with $N_0 = 10^{10}$ initial gamma-ray seeds emitted in that (L, H) position. The black line with the green region indicates the separation with the ground surface on Mt. Cimone, at about 2165 m a.s.l.

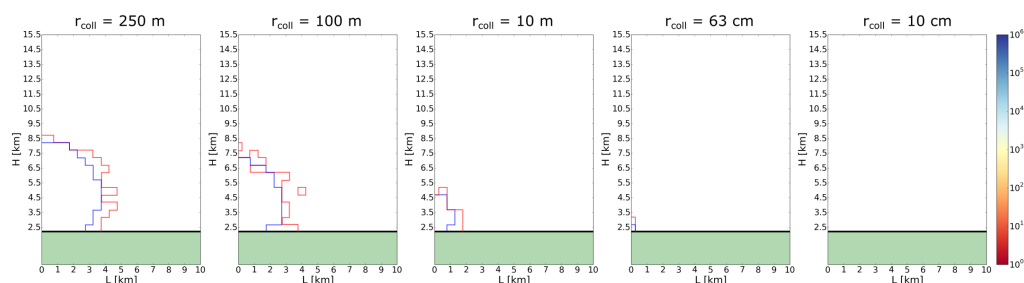


Figure 7. Comparison between the detectability regions obtained from the Geant4 numerical simulations (red contour) and from the analytical treatment (blue contour), for TGFs with an initial number of 10^{10} gamma-ray photons. Both approaches provide similar expected volumes around the Gamma-Flash detectors, from which TGFs can be detected, with a maximum discrepancy of ~ 1.5 km, due to the presence of statistical fluctuations in the Monte Carlo simulations.

5. Results

Given the good agreement between the results from Geant4 simulations and the analytical approach for $N_0 = 10^{10}$, we exploit the flexibility of the model to generate TGFs with $N_0 = 10^{18}$ initial seeds and evaluate the number of survived photons at the ground. Here, we adopted only the collecting area with $r_{coll} = 10$ cm, corresponding to the total equivalent geometric surface of the suite of Gamma-Flash gamma-ray detectors, placed inside the naval dome, and we limited the energy range to the 100 keV–10 MeV energy range, which is more consistent with the sensitivity of the detectors. Using these parameters, the analytical model provides a spatial extent of the detectability region around the detector ranging up to $L = 4.0$ km in ground distance and up to $H = 10.0$ km a.s.l. in altitude (corresponding to about 7.5 km above the installation site), as shown in the left panel of Figure 8. Although this study is mostly aimed at the identification of the spatial detectability regions, we provide a preliminary evaluation of the expected energy spectra of the survived TGF photons at ground, for different configuration, as shown in the right panel of Figure 8: here, we report the TGF spectra onground, at $L = 0.0$ km, and for different altitudes H , where the 100 keV–10 MeV energy range considered for the analysis is shaded in blue. Moreover, we point out that TGFs taking place nearby the detector (i.e., $L < 1.0$ km and $H < 4.5$ km) exhibit between 10^4 and 10^7 survived photons, resulting in extremely high fluxes. Taking into consideration that such fluxes are emitted within short-duration timescales on the order of tens of μs , TGFs occurring in this near region might saturate the detectors’ count rate.

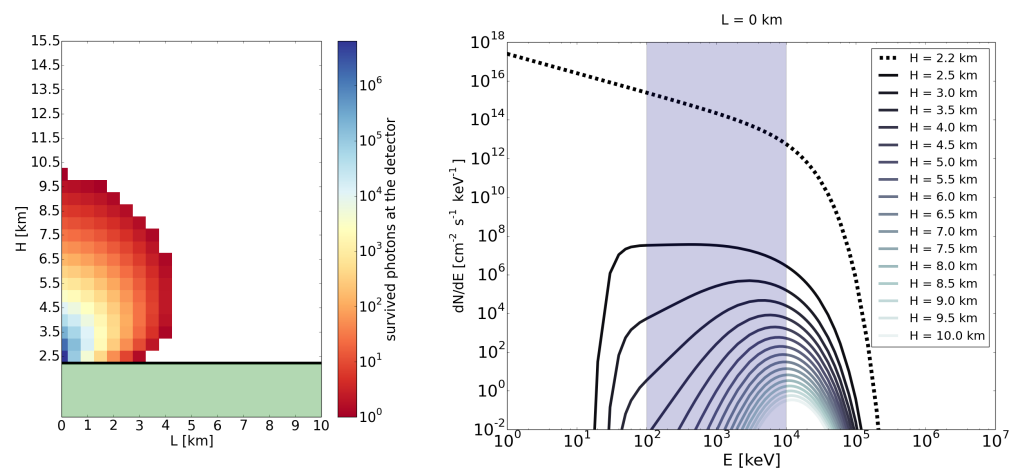


Figure 8. Left: detectability region obtained from the analytical model, for $N_0 = 10^{18}$ initial gamma-ray photons and emission half-angle $\alpha = 40^\circ$. TGF events occurring within this set of (L, H) values shall be detected on ground, by the mountain-based Gamma-Flash detection system. Right: spectra of the survived gamma-ray photons at the detector for different production altitudes H (here, only displayed for $L = 0.0$ km). The blue shaded region indicates the 100 keV–10 MeV energy range considered for the analysis.

5.1. Fraction of Survived Photons at Ground

We also evaluated the total fraction of TGF photons reaching the ground, out of $N_0 = 10^{18}$ initial seeds, by adopting a very large collecting surface of radius $r_{coll} = 5.0$ km. Such estimate ends up with a total fraction of survived photons equal to $\sim 10^{-6}$ out of those emitted at the source. This value is strongly model dependent, and it is about one order of magnitude smaller than that obtained by [40] using a RREA model, pointing out that, although providing a reliable spatial extent of the region from which TGFs can be detected, our analytical treatment may result in an underestimation of the amount of survived photons at ground.

5.2. Different Configurations

For completeness, we also investigated possible lower and higher intensity TGFs, with $N_0 = 10^{14}, 10^{15}, 10^{16}, 10^{17}, 10^{18}$, and 10^{19} initial seeds, respectively, as well as more collimated events with narrower emission half-angles $\alpha = 15^\circ, 30^\circ, 40^\circ$, and 60° . The results of this analysis are reported in Figure 9 and show that the size of the detectability region is proportional to the initial flux, with higher intensity TGFs detectable even at large distances from the target. In addition, tighter TGF emissions would make the gamma-ray photons inside the emission beam undergo less atmospheric attenuation, resulting in the detection of TGFs with larger numbers of survived photons. Nevertheless, even in the less favorable condition of $N_0 = 10^{14}$ seeds and $\alpha = 60^\circ$, TGFs occurring within a spatial region up to $L = 1.0$ km and $H = 4.0$ km a.s.l. shall exhibit a sufficient number of survived photons to be detected.

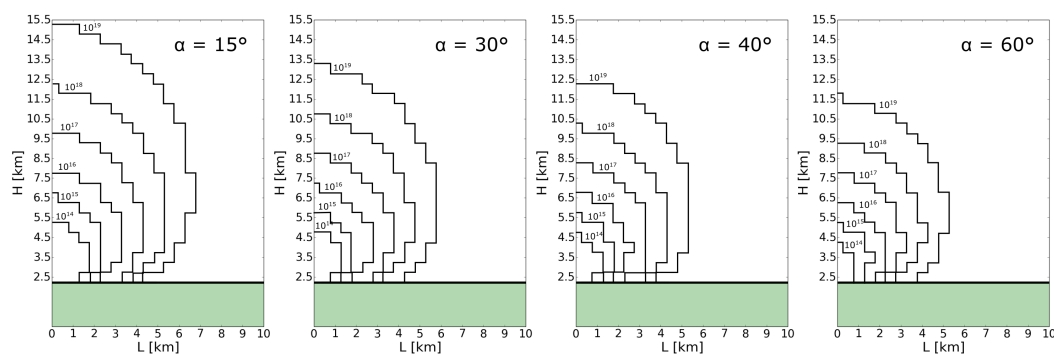


Figure 9. Detectability regions corresponding to TGFs with different initial numbers of seeds $N_0 = 10^{14}, 10^{15}, 10^{16}, 10^{17}, 10^{18}, 10^{19}$, and different emission half-angles $\alpha = 15^\circ, 30^\circ, 40^\circ, 60^\circ$. It can be noticed that the number of survived photons at the detector is proportional to the number of initial seeds N_0 and inversely proportional to the emission half-angle α .

6. Lightning Activity

If the mountain-based Gamma-Flash experiment can detect potential TGF emissions with different configurations, within different detectability regions in the surroundings of the installation site, it is fundamental to investigate the typical lightning occurrence in these spatial regions. We carried out such analysis by using the Lightning Network (LINET), a European wide lightning detection network, capable of revealing the radio signals (sferics) emitted by lightning strokes in the VLF/LF range (3–300 kHz), and of localizing the associated lightning flashes with a mean accuracy of ~ 75 m in a well deployed network and an overall average efficiency of ~ 4 kA (98%) [44]. The LINET network is capable of discriminating between Cloud-to-Ground (CG) and Intra-Cloud (IC) lightning, by means of the flash current intensity and the propagation delay among different stations. We analyzed the LINET sferics acquired in the time interval from 2012 to 2020, to obtain a statistics of the typical lightning occurrence at Mt. Cimone. We reconstructed the lightning density of CG and IC flashes and we evaluated the number of strokes occurring in the spatial region nearby the Gamma-Flash installation site. Figure 10 reports the yearly lightning density in the surroundings of the mountain-based Gamma-Flash experiment. The left panels report the CG (top) and IC (bottom) flash densities, with CG lightning strongly clustering at $L \sim 0$ km from the Gamma-Flash experiment and IC flashes mostly occurring at altitudes between $H \sim 5$ km and $H \sim 8$ km a.s.l. On the other hand, the right panel of Figure 10 shows the 2D flash density, where black contours mark the TGF detectability regions obtained in Section 5 for $\alpha = 40^\circ$ and different values of N_0 , and already reported in the left panel of Figure 8. It can be noticed that IC lightning flashes are more uniformly distributed in the surrounding space around the detectors, exhibiting density values ranging between 0.01 flashes $\text{km}^{-2} \text{y}^{-1}$ and 0.5 flashes $\text{km}^{-2} \text{y}^{-1}$. On the other hand, CG strokes strongly cluster nearby the Gamma-Flash experiment, where they reach up to more than 20 flashes $\text{km}^{-2} \text{y}^{-1}$ at $L = 0$ km: the larger CG lightning activity near the installation site is ascribed to orographic reasons and to the LINET detection efficiency.

We consider the different TGF configurations discussed in Figure 9, with half-angles $\alpha = 15^\circ, 30^\circ, 40^\circ$, and 60° and initial numbers of seeds $N_0 = 10^{14}, 10^{15}, 10^{16}, 10^{17}, 10^{18}$, and 10^{19} . Integrating the IC and CG lightning density in the detectability regions obtained for such configurations, we end up with the expected numbers of yearly flashes reported in Table 1, which range between 60 and 730 expected flashes in the regions of interest, depending on the configuration. We point out that: (1) not all these lightning discharges may emit TGFs; (2) not all the emitted TGFs may have a geometrical asset to be detected by the ground-based detectors. For what concerns the first point, we know that [35] reported an expected TGF-to-flash ratio on the order of 10^{-3} – 10^{-2} , which would make us expect about ~ 0.2 – 10 TGFs per year at the installation site. However, since such estimate comes from detections achieved from space, this value may be biased toward a particular sub-class of events with peculiar intensity and beaming characteristics, making the TGF-to-flash ratio

still a matter of debate. For what concerns the second point, a detailed treatment should take into consideration that lightning discharges could emit TGFs toward any direction, with only a fraction of them directed toward the detection system. In particular, if we assume that TGFs are generated at the lightning leader tip, events produced by CG flashes propagating to the ground are expected to be emitted toward a given direction out of a 2π hemisphere, whereas events produced by IC flashes propagating within the thundercloud may be emitted toward any direction out of a 4π sphere. However, for such treatment, two issues should be pointed out. First, the detectability regions in which we evaluate the amount of flashes are obtained by only considering the best case scenario in which TGFs are directed toward the detector. This introduces a bias, as for spatial positions near the installation site, even TGFs not directly pointing toward the detector may be revealed, and this translates in a larger fraction of solid angle out of 2π or 4π to be taken into account. Second, the lightning activity at Mt. Cimone is provided by LINET data, which does not have the same efficiency to IC and CG flashes, preventing us from obtaining a reliable discrimination between these two classes of events, and the associated fractions of solid angle in which TGFs may be emitted. Previsions of the expected number of TGFs at ground is a complex analysis and it is not the focus of our work. Nonetheless, our results demonstrate that the spatial region where typical TGFs can survive to the detectors is interested by a remarkable yearly lightning activity, making the ground-based Gamma-Flash installation site a suitable location for the aims of the program. A detailed treatment of the lightning activity at Mt. Cimone will be reported in (Tiberia et al., 2022, submitted).

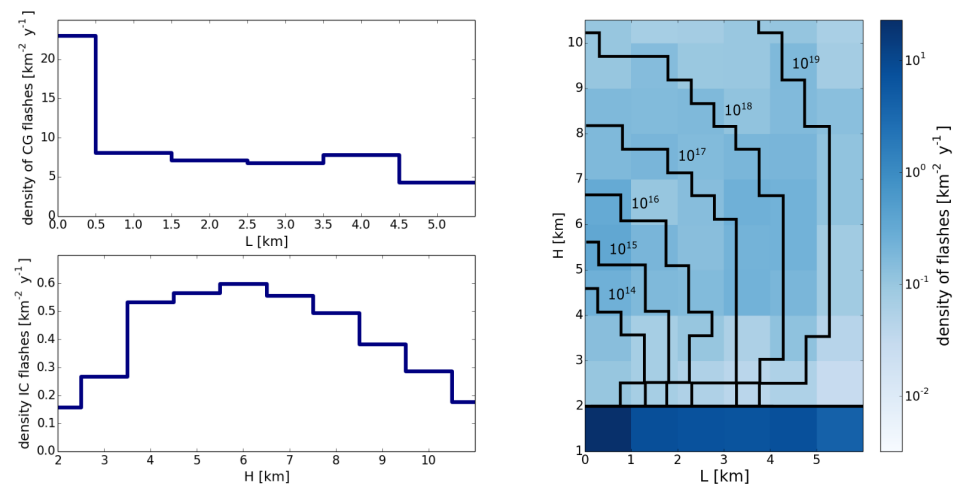


Figure 10. Left: CG (top) and IC (bottom) lightning flash density in the surroundings of the ground-based Gamma-Flash experiment on Mt. Cimone, obtained by LINET data acquired from 2012 to 2020. CG flashes strongly cluster at $L \sim 0$ km, due to orographic reasons, whereas IC lightning peaks at altitudes around $H \sim 6$ km a.s.l. Right: 2D lightning flash density, as a function of L and H . The black horizontal line at $H = 2$ km indicates the average ground elevation in the surroundings of the installation site on Mt. Cimone, marking the region where CG flashes take place. The black stepped contours represent the boundaries of the spatial regions in which TGFs can be detected by the ground-based Gamma-Flash experiment, obtained in Section 5 for $\alpha = 40^\circ$ and different values of N_0 .

Table 1. Expected yearly number of lightning discharges in the Gamma-Flash detectability regions.

	$N_0 = 10^{14}$	$N_0 = 10^{15}$	$N_0 = 10^{16}$	$N_0 = 10^{17}$	$N_0 = 10^{18}$	$N_0 = 10^{19}$
$\alpha = 15^\circ$	110	170	240	430	580	730
$\alpha = 30^\circ$	60	110	170	330	450	720
$\alpha = 40^\circ$	60	110	170	250	440	590
$\alpha = 60^\circ$	60	100	160	240	340	580

Expected yearly number of lightning strokes taking place within the detectability regions identified for different configurations of half-angle α and initial number of gamma-ray photons N_0 .

7. Conclusions

We investigated the detectability of TGFs by the Gamma-Flash ground-based experiment, installed at the Osservatorio Climatico “Ottavio Vittori” (CNR-ISAC) on Mt. Cimone (2165 m a.s.l.). We carried out Geant4 Monte Carlo simulations and a supporting numerical analytical treatment to identify a spatial region around the detectors, from which typical TGFs can survive and be detected with a sufficient high number of gamma-ray photons at the detector. For typical TGF events producing an initial number of 10^{18} photons within a emission half-angles of 40° , the analysis ended up identifying a “detectability region” extending up to $L = 4.0$ km distance on the ground from the Gamma-Flash detectors and up to $H = 10.0$ km height a.s.l. (corresponding to about 7.5 km above the installation site). If taking place at these positions, TGFs should be revealed by the Gamma-Flash detection system. We point out that even lower-intensity TGFs, emitting one order of magnitude less photons at the source, can be detected at the ground, although the corresponding detectability region would be significantly smaller. On the other hand, events exhibiting tighter beaming angles would result in higher fluxes at the detector. The detectable regions obtained by this study turn out to be compatible with the presence of frequent thunderstorm activity and lightning occurrence, as demonstrate by the analysis of the lightning sferics data acquired by the LINET network in the same geographic region. In particular, we expect that these detectable regions will be interested by 60–730 lightning flashes per year. From this study, we point out that the Gamma-Flash installation site is an ideal location to investigate thunderstorms and detect their associated high-energy emissions.

Author Contributions: Conceptualization, A.U.; methodology, A.U. and G.R.F.; software, A.U. and G.R.F.; validation, A.U. and G.R.F.; formal analysis, A.U.; investigation, A.U. and A.T.; resources, E.V. and M.T.; data curation, A.U., G.R.F. and A.T.; writing—original draft preparation, A.U.; writing—review and editing, A.U., E.A., E.P. and R.C.; supervision, E.V. and E.A.; project administration, E.V. and M.T. All authors have read and agreed to the published version of the manuscript.

Funding: This research received no external funding.

Data Availability Statement: The LINET data used in this work have been provided by CNR-ISAC, Rome.

Acknowledgments: Gamma-Flash is a mission of the Italian Space Agency (ASI), with programmatic and scientific participation of the National Institute for Astrophysics (INAF) and other research institutes and universities, supported by the ASI-INAF agreement N. 2020-5-HH.0. The authors thank the Institute of Atmospheric Sciences and Climate (ISAC) of the National Research Council (CNR) of Italy for the support to the Mt. Cimone CNR observatory and gratefully acknowledge the Italian Air Force Meteorological Service (Centro Aeronautico Militare di Montagna) for providing accessibility to the Mt. Cimone station. This work makes use of data of the Lightning NETWORK (LINET).

Conflicts of Interest: The authors declare no conflict of interest.

References

1. Gurevich, A.V.; Milikh, G.M.; Roussel-Dupre, R. Runaway electron mechanism of air breakdown and preconditioning during a thunderstorm. *Phys. Lett. A* **1992**, *165*, 463–468. [[CrossRef](#)]
2. Dwyer, J.R.; Uman, M.A.; Rassoul, H.K.; Al-Dayeh, M.; Caraway, L.; Jerauld, J.; Rakov, V.A.; Jordan, D.M.; Rambo, K.J.; Corbin, V.; et al. Energetic Radiation Produced During Rocket-Triggered Lightning. *Science* **2003**, *299*, 694–697. [[CrossRef](#)] [[PubMed](#)]
3. Smith, D.M.; Dwyer, J.R.; Hazelton, B.J.; Grefenstette, B.W.; Martinez-McKinney, G.F.M.; Zhang, Z.Y.; Lowell, A.W.; Kelley, N.A.; Splitt, M.E.; Lazarus, S.M.; et al. A terrestrial gamma ray flash observed from an aircraft. *J. Geophys. Res.* **2011**, *116*, 20124. [[CrossRef](#)]
4. Bowers, G.S.; Smith, D.M.; Kelley, N.A.; Martinez-McKinney, G.F.; Cummer, S.A.; Dwyer, J.R.; Heckman, S.; Holzworth, R.H.; Marks, F.; Reasor, P.; et al. A Terrestrial Gamma-Ray Flash inside the Eyewall of Hurricane Patricia. *J. Geophys. Res.* **2018**, *123*, 4977–4987. [[CrossRef](#)]
5. Tran, M.D.; Rakov, V.A.; Mallick, S.; Dwyer, J.R.; Nag, A.; Heckman, S. A terrestrial gamma-ray flash recorded at the Lightning Observatory in Gainesville, Florida. *J. Atmos. Sol. Terr. Phys.* **2015**, *136*, 86–93. [[CrossRef](#)]
6. Abbasi, R.U.; Abu-Zayyad, T.; Allen, M.; Barcikowski, E.; Belz, J.W.; Bergman, D.R.; Blake, S.A.; Byrne, M.; Cady, R.; Cheon, B.; et al. Gamma Ray Showers Observed at Ground Level in Coincidence with Downward Lightning Leaders. *J. Geophys. Res. Atmos.* **2018**, *123*, 6864–6879. [[CrossRef](#)]

7. Enoto, T.; Wada, Y.; Furuta, Y.; Nakazawa, K.; Yuasa, T.; Okuda, K.; Makishima, K.; Sato, M.; Sato, Y.; Nakano, T.; et al. Photonuclear reactions triggered by lightning discharge. *Nature* **2017**, *551*, 481–484. [[CrossRef](#)]
8. Bowers, G.S.; Smith, D.M.; Martinez-McKinney, G.F.; Kamogawa, M.; Cummer, S.A.; Dwyer, J.R.; Wang, D.; Stock, M.; Kawasaki, Z. Gamma Ray Signatures of Neutrons From a Terrestrial Gamma Ray Flash. *Geophys. Res. Lett.* **2017**, *44*, 10. [[CrossRef](#)]
9. Pleshinger, D.J.; Alnussirat, S.T.; Arias, J.; Bai, S.; Banadaki, Y.; Cherry, M.L.; Hoffman, J.H.; Khosravi, E.; Legault, M.D.; Rodriguez, R.; et al. Gamma Ray Flashes Produced by Lightning Observed at Ground Level by TETRA-II. *J. Geophys. Res.* **2019**, *124*, 9229–9238. [[CrossRef](#)]
10. Wada, Y.; Enoto, T.; Nakazawa, K.; Furuta, Y.; Yuasa, T.; Nakamura, Y.; Morimoto, T.; Matsumoto, T.; Makishima, K.; Tsuchiya, H. Downward Terrestrial Gamma-Ray Flash Observed in a Winter Thunderstorm. *Phys. Rev. Lett.* **2019**, *123*, 061103. [[CrossRef](#)]
11. Belz, J.W.; Krehbiel, P.R.; Remington, J.; Stanley, M.A.; Abbasi, R.U.; LeVon, R.; Rison, W.; Rodeheffer, D.; Abu-Zayyad, T.; Allen, M.; et al. Observations of the Origin of Downward Terrestrial Gamma-Ray Flashes. *J. Geophys. Res.* **2020**, *125*, e31940. [[CrossRef](#)]
12. Dwyer, J.R.; Rassoul, H.K.; Al-Dayeh, M.; Caraway, L.; Wright, B.; Chrest, A.; Uman, M.A.; Rakov, V.A.; Rambo, K.J.; Jordan, D.M.; et al. A ground level gamma-ray burst observed in association with rocket-triggered lightning. *Geophys. Res. Lett.* **2004**, *31*, L05119. [[CrossRef](#)]
13. Hare, B.M.; Uman, M.A.; Dwyer, J.R.; Jordan, D.M.; Biggerstaff, M.I.; Caicedo, J.A.; Carvalho, F.L.; Wilkes, R.A.; Kotovsky, D.A.; Gameraota, W.R.; et al. Ground-level observation of a terrestrial gamma ray flash initiated by a triggered lightning. *J. Geophys. Res.* **2016**, *121*, 6511–6533. [[CrossRef](#)]
14. Smith, D.M.; Bowers, G.S.; Kamogawa, M.; Wang, D.; Ushio, T.; Ortberg, J.; Dwyer, J.R.; Stock, M. Characterizing Upward Lightning With and Without a Terrestrial Gamma Ray Flash. *J. Geophys. Res.* **2018**, *123*, 11321–11332. [[CrossRef](#)]
15. Ortberg, J.; Smith, D.M.; Li, J.; Dwyer, J.; Bowers, G. Detecting an Upward Terrestrial Gamma Ray Flash from its Reverse Positron Beam. *J. Geophys. Res.* **2020**, *125*, e30942. [[CrossRef](#)]
16. Pu, Y.; Cummer, S.A.; Huang, A.; Briggs, M.; Mailyan, B.; Lesage, S. A Satellite-Detected Terrestrial Gamma Ray Flash Produced by a Cloud-to-Ground Lightning Leader. *Geophys. Res. Lett.* **2020**, *47*, e89427. [[CrossRef](#)]
17. Torii, T.; Takeishi, M.; Hosono, T. Observation of gamma-ray dose increase associated with winter thunderstorm and lightning activity. *J. Geophys. Res.* **2002**, *107*, 4324. [[CrossRef](#)]
18. Chilingarian, A.; Daryan, A.; Arakelyan, K.; Hovhannisyanyan, A.; Mailyan, B.; Melkumyan, L.; Hovsepnyan, G.; Chilingaryan, S.; Reymers, A.; Vanyan, L. Ground-based observations of thunderstorm-correlated fluxes of high-energy electrons, gamma rays, and neutrons. *Phys. Rev. D* **2010**, *82*, 043009. [[CrossRef](#)]
19. Tsuchiya, H.; Enoto, T.; Yamada, S.; Yuasa, T.; Kawaharada, M.; Kitaguchi, T.; Kokubun, M.; Kato, H.; Okano, M.; Nakamura, S.; et al. Detection of High-Energy Gamma Rays from Winter Thunderclouds. *Phys. Rev. Lett.* **2007**, *99*, 165002. [[CrossRef](#)]
20. Tsuchiya, H.; Enoto, T.; Yamada, S.; Yuasa, T.; Nakazawa, K.; Kitaguchi, T.; Kawaharada, M.; Kokubun, M.; Kato, H.; Okano, M.; et al. Long-duration γ ray emissions from 2007 and 2008 winter thunderstorms. *J. Geophys. Res.* **2011**, *116*, D09113. [[CrossRef](#)]
21. Chilingarian, A.; Bostanjyan, N.; Vanyan, L. Neutron bursts associated with thunderstorms. *Phys. Rev. D* **2012**, *85*, 085017. [[CrossRef](#)]
22. Tsuchiya, H.; Hibino, K.; Kawata, K.; Hotta, N.; Tateyama, N.; Ohnishi, M.; Takita, M.; Chen, D.; Huang, J.; Miyasaka, M.; et al. Observation of thundercloud-related gamma rays and neutrons in Tibet. *Phys. Rev. D* **2012**, *85*, 092006. [[CrossRef](#)]
23. Alekseenko, V.; Arneodo, F.; Bruno, G.; Di Giovanni, A.; Fulgione, W.; Gromushkin, D.; Shchegolev, O.; Stenkin, Y.; Stepanov, V.; Sulakov, V.; et al. Decrease of Atmospheric Neutron Counts Observed during Thunderstorms. *Phys. Rev. Lett.* **2015**, *114*, 125003. [[CrossRef](#)] [[PubMed](#)]
24. Tavani, M.; Barbiellini, G.; Argan, A.; Boffelli, F.; Bulgarelli, A.; Caraveo, P.; Cattaneo, P.W.; Chen, A.W.; Cocco, V.; Costa, E.; et al. The AGILE Mission. *Astron. Astrophys.* **2009**, *502*, 995–1013. [[CrossRef](#)]
25. Marisaldi, M.; Fuschino, F.; Labanti, C.; Galli, M.; Longo, F.; Del Monte, E.; Barbiellini, G.; Tavani, M.; Giuliani, A.; Moretti, E.; et al. Detection of terrestrial gamma ray flashes up to 40 MeV by the AGILE satellite. *J. Geophys. Res.* **2010**, *115*. [[CrossRef](#)]
26. Tavani, M.; Marisaldi, M.; Labanti, C.; Fuschino, F.; Argan, A.; Trois, A.; Giommi, P.; Colafrancesco, S.; Pittori, C.; Palma, F.; et al. Terrestrial Gamma-Ray Flashes as Powerful Particle Accelerators. *Phys. Rev. Lett.* **2011**, *106*, 018501. [[CrossRef](#)]
27. Tavani, M.; Argan, A.; Paccagnella, A.; Pesoli, A.; Palma, F.; Gerardin, S.; Bagatin, M.; Trois, A.; Picozza, P.; Benvenuti, P.; et al. Possible effects on avionics induced by terrestrial gamma-ray flashes. *Nat. Hazards Earth Syst. Sci.* **2013**, *13*, 1127–1133. [[CrossRef](#)]
28. Marisaldi, M.; Argan, A.; Ursi, A.; Gjesteland, T.; Fuschino, F.; Labanti, C.; Galli, M.; Tavani, M.; Pittori, C.; Verrecchia, F.; et al. Enhanced detection of terrestrial gamma-ray flashes by AGILE. *Geophys. Res. Lett.* **2015**, *42*, 9481–9487. [[CrossRef](#)]
29. Ursi, A.; Marisaldi, M.; Tavani, M.; Casella, D.; Sandò, P.; Dietrich, S. Detection of multiple terrestrial gamma-ray flashes from thunderstorm systems. *J. Geophys. Res.* **2016**, *121*, 11. [[CrossRef](#)]
30. Ursi, A.; Guidorzi, C.; Marisaldi, M.; Sarria, D.; Frontera, F. Terrestrial gamma-ray flashes in the BeppoSAX data archive. *J. Atmos. Sol. Terr. Phys.* **2017**, *156*, 50–56. [[CrossRef](#)]
31. Marisaldi, M.; Galli, M.; Labanti, C.; Østgaard, N.; Sarria, D.; Cummer, S.A.; Lyu, F.; Lindanger, A.; Campana, R.; Ursi, A.; et al. On the High-Energy Spectral Component and Fine Time Structure of Terrestrial Gamma Ray Flashes. *J. Geophys. Res.* **2019**, *124*, 7484–7497. [[CrossRef](#)]

32. Lindanger, A.; Marisaldi, M.; Maiorana, C.; Sarria, D.; Albrechtsen, K.; Østgaard, N.; Galli, M.; Ursi, A.; Labanti, C.; Tavani, M.; et al. The 3rd AGILE Terrestrial Gamma Ray Flash Catalog. Part I: Association to Lightning Sferics. *J. Geophys. Res. Atmos.* **2020**, *125*, e2019JD031985. [[CrossRef](#)]
33. Maiorana, C.; Marisaldi, M.; Lindanger, A.; Østgaard, N.; Ursi, A.; Sarria, D.; Galli, M.; Labanti, C.; Tavani, M.; Pittori, C.; et al. The 3rd AGILE Terrestrial Gamma-ray Flashes Catalog. Part II: Optimized Selection Criteria and Characteristics of the New Sample. *J. Geophys. Res. Atmos.* **2020**, *125*, e2019JD031986. [[CrossRef](#)]
34. Arnone, E.; Bór, J.; Chanrion, O.; Barta, V.; Dietrich, S.; Enell, C.F.; Farges, T.; Füllekrug, M.; Kero, A.; Labanti, R.; et al. Climatology of Transient Luminous Events and Lightning Observed Above Europe and the Mediterranean Sea. *Surv. Geophys.* **2019**, *41*, 167–199. [[CrossRef](#)]
35. Smith, D.M.; Dwyer, J.R.; Hazelton, B.J.; Grefenstette, B.W.; Martinez-McKinney, G.F.M.; Zhang, Z.Y.; Lowell, A.W.; Kelley, N.A.; Splitt, M.E.; Lazarus, S.M.; et al. The rarity of terrestrial gamma-ray flashes. *Geophys. Res. Lett.* **2011**, *38*. [[CrossRef](#)]
36. Østgaard, N.; Gjesteland, T.; Hansen, R.S.; Collier, A.B.; Carlson, B. The true fluence distribution of terrestrial gamma flashes at satellite altitude. *J. Geophys. Res.* **2012**, *117*, 3327. [[CrossRef](#)]
37. Gjesteland, T.; Østgaard, N.; Collier, A.B.; Carlson, B.E.; Cohen, M.B.; Lehtinen, N.G. Confining the angular distribution of terrestrial gamma ray flash emission. *J. Geophys. Res.* **2011**, *116*, A11313. [[CrossRef](#)]
38. Minzner, R.A. The 1976 Standard Atmosphere and its relationship to earlier standards. *Rev. Geophys.* **1977**, *15*, 375–384. [[CrossRef](#)]
39. Dwyer, J.R.; Smith, D.M. A comparison between Monte Carlo simulations of runaway breakdown and terrestrial gamma-ray flash observations. *Geophys. Res. Lett.* **2005**, *32*, 22804. [[CrossRef](#)]
40. Berge, N.; Celestin, S. Constraining Downward Terrestrial Gamma Ray Flashes Using Ground-Based Particle Detector Arrays. *Geophys. Res. Lett.* **2019**, *46*, 8424–8430. [[CrossRef](#)]
41. Agostinelli, S.; Allison, J.; Amako, K.A.; Apostolakis, J.; Araujo, H.; Arce, P.; Asai, M.; Axen, D.; Banerjee, S.; Barrand, G.; et al. Geant4—A simulation toolkit. *Nucl. Instr. Meth. A* **2003**, *506*, 250–303. [[CrossRef](#)]
42. Allison, J.; Amako, K.; Apostolakis, J.; Araujo, H.; Arce, P.; Asai, M.; Barrand, G.; Capra, R.; Chauvie, S.; Chytracsek, R.; et al. Geant4 Developments and Applications. *IEEE Trans. Nucl. Sci.* **2006**, *53*, 270–278. [[CrossRef](#)]
43. Allison, J.; Amako, K.; Apostolakis, J.; Arce, P.; Asai, M.; Aso, T.; Bagli, E.; Bagulya, A.; Banerjee, S.; Barrand, G.; et al. Recent developments in Geant4. *Nucl. Instrum. Methods Phys. Res. Sect. A Accel. Spectrometers Detect. Assoc. Equip.* **2016**, *835*, 186–225. [[CrossRef](#)]
44. Betz, H.; Schmidt, K.; Laroche, P.; Blanchet, P.; Oettinger, W.; Defer, E.; Dziewit, Z.; Konarski, J. LINET—An international lightning detection network in Europe. *Atmos. Res.* **2009**, *91*, 564–573. [[CrossRef](#)]